Available online at website: https://journal.bcrec.id/index.php/bcrec

Bulletin of Chemical Reaction Engineering & Catalysis, 19 (4) 2024, 548-559

Research Article

Synthesis of $MgFe_2O_4$ Nanoparticles and its Application for Photodegradation of Methylene Blue

Dede Sukandar[1*], Adawiah Adawiah[1], Saeful Rohman[2], Shella Fitria[1], Nanda Saridewi[3], Salman Farishi[4], Nurhasni Nurhasni[1], Isalmi Aziz[1], Yulyani Nur Azizah[1]

[1]Department of Chemistry, Faculty of Science and Technology, UIN Syarif Hidayatullah Jakarta, Jl. Ir. H. Juanda No. 95 Ciputat Tangerang Selatan 15412, Indonesia
[2]Research Center for Advanced Materials, National Research and Innovation Agency, KST BJ Habibie, South Tangerang 15314, Indonesia
[3]Department of Chemistry Education, Faculty of Tarbiya and Teaching Sciences, UIN Syarif Hidayatullah, Jl. Ir. H. Juanda No. 95 Ciputat Tangerang Selatan 15412, Indonesia
[4]Research Centre for Polymer Technology, National Research and Innovation Agency, Gedung 460, Kawasan Puspitek Serpong, Muncul, Kec. Setu, Kota Tangerang Selatan, Banten 15314

Received: 30th September 2024; Revised: 21th October 2024; Accepted: 22th October 2024
Available online: 29th October 2024; Published regularly: December 2024

Abstract

Methylene blue wastewater from the paper, clothing, and textile industries can adversely affect aquatic ecosystems if improperly treated. One method to treat methylene blue pollutants in sewage is through photocatalysis techniques using magnesium ferrite ($MgFe_2O_4$) nanoparticle-based semiconductors. The $MgFe_2O_4$ is effective for methylene blue degradation because it is stable in aqueous systems, inexpensive, and has good photocatalytic activity. This study aims to synthesize $MgFe_2O_4$ nanoparticles with pumpkin seed extract (*Cucurbita moschata*) as a capping agent through a hydrothermal method. Characterization results show that $MgFe_2O_4$ nanoparticles synthesized with the addition of 3 mL pumpkin seed extract have a crystal size of 3.87 nm, cubic spinel structure, average particle size of 29 nm, and band gap energy value of 1.94 eV. The $MgFe_2O_4$ nanoparticles produced optimum degradation efficiency under mercury lamp irradiation with a degradation capacity of 391.98 mg/g at pH = 12.

Keywords: hydrothemal; photocatalyst; methylene blue; $MgFe_2O_4$ nanoparticles

How to Cite: Sukandar, D., Adawiah, A., Rohman, S., Fitria, S., Saridewi, N., Farishi, S., Nurhasni, N., Aziz, I., & Azizah, Y.N. (2024). Synthesis of $MgFe_2O_4$ Nanoparticles and its Application for Photodegradation of Methylene Blue. *Bulletin of Chemical Reaction Engineering & Catalysis*, 19 (4), 548-559 (doi: 10.9767/bcrec.20222)

Permalink/DOI: https://doi.org/10.9767/bcrec.20222

1. Introduction

The wastewater from the textile industry contains a wide variety of pollutants that are harmful to the environmental ecosystem, including organic matter, inorganics, heavy metals, and dyes [1]. The textile industry uses 1000 100,000 kinds of dyes, which are available in the commercial market. Based on data from Badan Pusat Statistik, Indonesia's average import volume of synthetic dyes in the last five years has reached more than 42,000 tons/year [2]. Methylene blue is one of the dyes with the highest consumption rate in the textile industry [3].

Methylene blue is widely applied in the textile industry because it contains many chromophore groups, so it has an intense colour attachment to fabric, cotton, and paper fibres [4-5]. Methylene blue is classified as a heterocyclic aromatic chemical compound and is difficult to degrade naturally [6]. The presence of methylene blue in high concentrations has harmful effects on aquatic ecosystems. In addition, methylene blue contaminated water, when consumed, can cause

* Corresponding Author.
Email: sukandarkimia@uinjkt.ac.id (D. Sukandar)

cyanosis, necrosis, and increased heart rate in humans [7-8]. Several treatment methods have been used to address the pressing environmental issues caused by dye waste, including coagulation-flocculation, biodegradation, chlorination, and filtration [9-11]. However, these methods, while useful, have their limitations in fully eliminating the dye waste, necessitating further treatment [12]. This underscores the urgent need for a more effective solution. One such promising method is the use of photocatalysis techniques, which can break down the dye into smaller, safer components through photodegradation reactions [13].

Photocatalysis is a chemical transformation process involving photons (light) as an energy source and catalyst to increase the rate of transformation [14]. The application of dye waste treatment using this method has advantages; namely, the reaction results do not require further processing, are simple, economical, and can convert pollutants into degradation products with lower toxicity [15-16]. The photocatalysis method requires semiconductor materials in nanoparticles with chemically stable characteristics and high photocatalytic activity and can be used repeatedly [17].

One type of photocatalyst that can be applied for dye photodegradation is metal ferrite (MFe_2O_4) [18-19]. MFe_2O_4 is a ferrite compound with M as a divalent metal ion that can be used in the degradation process, such as Mn, Fe, Cu, Ni, Mg, and Co [20]. Magnesium ferrite ($MgFe_2O_4$) is one of the most effective ferrite compounds used for photodegradation of dye pollutants because it has good photocatalytic activity and stability in aqueous media [21]. In addition, $MgFe_2O_4$ has a reasonably small band gap energy (~1.9 eV), is easy to synthesize at a low cost, and is non-toxic [22-24].

MFe_2O_4 nanoparticles can be synthesized using various methods, such as sol-gel, sonochemical, co-precipitation, and hydrothermal methods [25-29]. However, the most effective method is hydrothermal, a method with great potential, due to its environmental friendliness and economy. The product has high crystallinity, a key factor in its function as a photocatalyst, and can produce nano-sized particles [28]. Saridewi *et al*. (2024) successfully synthesized ferrite metal nanoparticles in the form of $ZnFe_2O_4$ through a hydrothermal method, a promising approach, to produce a particle size of 26.15 nm with the addition of 3 mL of Lidah mertua extract [28].

In recent years, researchers have focused on using eco-friendly synthesis methods to minimize dependence on harmful synthetic chemicals. This method involves using environmentally safe materials sourced from plant extracts. Plant extracts can serve as capping and stabilizer agents in nanoparticle synthesis because they contain secondary metabolite compounds for forming metal and metal oxide nanostructures.

Pumpkin seeds (*Curcubita moschata*) are one of the potential materials used as a capping agent in nanoparticle synthesis. The phytochemical content in pumpkin seeds in the form of flavonoid and polyphenol compounds acts as a capping agent in nanoparticle synthesis [25]. Flavonoids play a role in preventing nanoparticle agglomeration and can control particle growth by reducing surface energy in preventing aggregation [30-31]. Saridewi *et al*. successfully synthesized ZnO nanoparticles with pumpkin seed extract through the sol-gel method, showing a spherical shape with an average particle size of 28.07 nm [25].

According to the literature investigation, the utilization of plant extracts in the synthesis process of metal ferrite nanoparticles, particularly based on magnesium metal and its application as a photocatalyst, is still difficult to find. Based on this background, this research focuses on synthesising magnesium ferrite nanoparticle-based photocatalyst ($MgFe_2O_4$) through a hydrothermal method using pumpkin seed extract (*C. moschata*) as a capping agent. Determination of $MgFe_2O_4$ performance as a photocatalyst was carried out by measuring the degradation efficiency of $MgFe_2O_4$ against methylene blue dye under 250-watt mercury lamp irradiation for 1 hour. Optimization was carried out on the variation of pH, methylene blue concentration, and $MgFe_2O_4$ mass.

2. Materials and Methods

2.1 Materials

The materials used in this study were dried pumpkin seeds (*C. moschata*) obtained from the Yogyakarta area, sodium hydroxide (NaOH) emsure grade (Merck), magnesium nitrate hexahydrate ($Mg(NO_3)_2.6H_2O$) (p.a) (Merck), iron(III) nitrate nonahydrate ($Fe(NO_3)_3.9H_2O$) (p.a.) (Merck) distilled water, and methylene blue (Merck).

2.2 Synthesis of $MgFe_2O_4$ Nanoparticles

Pumpkin seeds (*C. moschata*) were dried at 100 °C for two days. Next, the dried seeds were pulverized into powder. 5.0 g of pumpkin seed powder was put into a beaker, and 100 mL of distilled water was added. After that, it was heated in a 58 °C water bath for two hours while stirring using a magnetic stirrer at 300 rpm. The pumpkin seed extract was filtered with Whatman No. 41 paper, and the filtrate was then used in the $MgFe_2O_4$ nanoparticle synthesis process.

The $MgFe_2O_4$ nanoparticles were synthesised hydrothermally with a capping agent in pumpkin

seed extract (*C. moschata*). A total of 0.005 mol $Mg(NO_3)_2.6H_2O$ and 0.01 mol $Fe(NO_3)_3.9H_2O$ were dissolved with 17 mL of distilled water and stirred using a magnetic stirrer at 500 rpm. Next, 3 mL of pumpkin seed extract was added to the mixture while continuing to stir. After that, stirring was continued for 1 hour. Next, 4 M NaOH was added until pH = 12 and stirred again for 2 hours. The mixture was then put into a Teflon-line autoclave and heated at 180 °C for 3 hours. The precipitate formed was filtered and washed using distilled water until pH = 7. The precipitate was dried at 110 °C for 4 hours, then calcined at 500 °C for 2 hours to produce $MgFe_2O_4$ powder.

2.3 Characterization of $MgFe_2O_4$ Nanoparticles

The crystallinity and crystal size of $MgFe_2O_4$ nanoparticles were analyzed using a Shimadzu XRD 7000 Maxima X-ray diffraction (XRD) using Cu-Kα radiation (λ = 1.54056 Å) at 40 kV voltage and 30 mA current. The diffractograms were processed through the Origin application to determine sample size, crystallinity, and phase type. The Debye Scherrer equation (Equation 1) determined the crystal size.

$$D = \frac{k\lambda}{\beta cos\,\theta} \quad (1)$$

where, D is crystal size, k is crystal form factor (0.9), λ is X-ray wavelength (λ = 1.5418 Å), β is value of Full Width at Half (FWHM) (rad), and θ is diffraction angle (degree).

The surface morphology of $MgFe_2O_4$ nanoparticles was analyzed using an FEI Quanta 650 SEM at a voltage of 25 kV. Ultraviolet-Visible Diffuse Reflectance Spectroscopy (UV-Vis DRS) measurements were carried out to determine the sample's band gap energy based on the measurement of light intensity reflected by the sample. Reflectance measurements were made in the 200-800 nm region using $BaSO_4$ powder as a blank. The Kubelka-Munk equation (Equation 2) determined the band gap energy.

$$\frac{K}{S} = \frac{(1-R)^2}{2R} = F(R) \quad (2)$$

where, R is the diffuse reflectance and $F(R)$ is called the Kubelka-Munk function.

In a parabolic band structure, the band gap energy (E_g) and absorption coefficient (α) values are connected through the Tauc plot. The Tauc relationship for band gap energy is shown in Equation (3).

$$\alpha(h\upsilon) \approx A\left(h\upsilon - E_g\right)^n \quad (3)$$

where, α is linear absorption coefficient, υ is light frequency ($\upsilon = c/\lambda$, s^{-1}), A is proportionality constant, h is Planck constant (6.626×10^{-34} J.s), E_g is band gap energy (eV), and n is allowed electronic transition value (n = 2 for indirect transition, n = ½ for direct transition). When the incident radiation is perfectly scattered, the absorption coefficient K equals 2α. In this case, considering the scattering coefficient S as constant to wavelength, the Kubelka Munk function is proportional to the absorption coefficient α; using Equation (2), we get the relation (Equation 4):

$$[F(R)h\upsilon]^{1/n} = A\left(h\upsilon - E_g\right) \quad (4)$$

Furthermore, the band gap is calculated by plotting the graph of $[F(R)h\upsilon]^{1/n}$ as the y-axis and energy ($h\upsilon$) as the x-axis. The band gap can be obtained by extending a straight line from a straight graph part connecting the x-axis ($h\upsilon$). The value of the band gap is the energy (hv) when $[F(R)h\upsilon]^{1/n}$ is equal to zero.

2.4 Photocatalytic Activity Test of $MgFe_2O_4$

The photocatalytic activity of $MgFe_2O_4$ nanoparticles for methylene blue degradation was tested at variations of pH (6-13), methylene blue concentration (10-80 ppm), and $MgFe_2O_4$ mass (5-25 mg). The photocatalytic activity test was conducted under 250-watt mercury lamp irradiation for 1 hour. The test was performed by dispersing $MgFe_2O_4$ nanoparticles into 50 mL of methylene blue solution. Furthermore, the suspension was magnetically stirred at 300 rpm. The suspension was then sampled as much as 2 mL and centrifuged at 6000 rpm for 10 minutes. The absorbance of methylene blue in the solution was measured using a UV-Vis spectrophotometer at 665 nm. The degradation efficiency and degradation capacity of methylene blue were determined by the following Equations 5 and 6:

$$Degradation\ efficiency\ (\%) = \frac{(C_0 - C_t)}{C_0} \times 100\% \quad (5)$$

$$Q = Degradation\ efficiency\ (\%) \times C_0 \times \frac{V}{m} \quad (6)$$

where, C_0 is initial concentration of methylene blue (mg/L) (t = 0 min), Ct is methylene blue concentration at a certain reaction time, Q is degradation capacity (mg/g), m is mass of photocatalyst (gram), and V is methylene blue solution volume (L).

3. Results and Discussion

3.1 $MgFe_2O_4$ Nanoparticles

$MgFe_2O_4$ nanoparticles were synthesized using a hydrothermal method that involves the process of crystal formation through a reaction mechanism between $Mg(NO_3)_2.6H_2O$ and $Fe(NO_3)_3.9H_2O$ solutions with pumpkin seed

extract (*C. moschata*) as a capping agent and the addition of NaOH as a strong base that plays a role in the crystallization process. The hydrothermal stimulate crystal growth during mineralization, with the reaction taking place in a secure closed system using water as a solvent at 180 °C and high pressure [29,32]. Temperature is one factor affecting the formation of the $MgFe_2O_4$ crystal phase; if the temperature is below 180 °C, the reaction is not entirely successful. The water acts as a solvent accelerate the reaction and changing the physical and chemical properties of products and reactants [33]. Hydrolysis and ionization reactions will increase with increasing temperature and pressure, and the crystallization process occurs when the dielectric constant of water decreases with increasing temperature and pressure.

Rohmah *et al*. [34] explained that the addition of NaOH initiates the nucleation process by catalyzing the hydration reaction of the metal hydroxide mixture, thus forming a precipitate by increasing the rate of nucleation and crystal growth and ensuring faster and more controllable crystal growth. NaOH plays an essential role in the synthesis of $MgFe_2O_4$ by controlling the pH of the solution, which is crucial for precipitating Mg^{2+} and Fe^{3+} ions in the form of hydroxides. As a precipitating agent OH^- ions react with Mg^{2+} and Fe^{3+} ions to form $Mg(OH)_2$, $Fe(OH)_3$ and $Mg_xFe_y(OH)_z$ precipitates. Thus, the $Mg_xFe_y(OH)_z$ was washed using distilled water to remove impurities or contaminants in $MgFe_2O_4$ so that the resulting $MgFe_2O_4$ crystal has high purity. These impurities are from excess NaOH and NO_3^- ions. The drying process is carried out at 110 °C to remove solvents still trapped in the $Mg_xFe_y(OH)_z$. The calcination process is carried out at 500 °C for two hours to convert $Mg_xFe_y(OH)_z$ into $MgFe_2O_4$ crystals.

NaOH concentration is essential in controlling the size of $MgFe_2O_4$ particles formed. Puspitasari et al. have successfully synthesized $MnFe_2O_4$ nanoparticles with the addition of NaOH at pH = 12, resulting in a smaller crystal size of $MnFe_2O_4$ nanoparticles compared to NaOH pH = 10, namely 11.0564 nm [35]. The $MgFe_2O_4$ synthesis reaction can generally be seen in Equations (6-12).

$$Mg(NO_3)_2.6H_2O_{(aq)} \rightarrow Mg^{2+}{}_{(aq)} + NO_3^-{}_{(aq)} + 2H_2O_{(l)} \quad (7)$$

$$Fe(NO_3)_3.9H_2O_{(aq)} \rightarrow Fe^{3+}{}_{(aq)} + 3NO_3^-{}_{(aq)} + 9H_2O_{(1)} \quad (8)$$

$$Mg^{2+}{}_{(aq)} + 2OH^-{}_{(aq)} \rightarrow Mg(OH)_{2(s)} \quad (9)$$

$$Fe^{3+}{}_{(aq)} + 3OH^-{}_{(aq)} \rightarrow Fe(OH)_{3(s)} \quad (10)$$

$$Mg^{2+}{}_{(aq)} + Fe^{3+}{}_{(aq)} + OH^-{}_{(aq)} \rightarrow Mg_xFe_y(OH)_{z\,(s)} \quad (11)$$

$$Mg_xFe_y(OH)_{z(s)} \xrightarrow{\Delta} MgFe_2O_{4(s)} + H_2O_{(g)} \quad (12)$$

Pumpkin (*C. moschata*) seed extract acts as a capping agent to form a protective layer by binding to the nanoparticle surface and selectively affecting the nanoparticle structure to prevent aggregation. The polyphenol compounds in pumpkin seed extra plays in forming the Mg/Fe-polyphenol complex compound. The negatively charged hydroxyl groups from those compounds reduce Mg^{2+} and Fe^{3+} to Mg and Fe. Then, the Mg and Fe atoms formed into Mg and Fe clusters, and prevent aggregation between Mg and Fe clusters, thus forming stable nanoparticles [36]. The synthesis mechanism of $MgFe_2O_4$ nanoparticles using pumpkin seed extract is shown below (Figure 1).

Figure 2 shows the results of synthesising powder-shaped $MgFe_2O_4$ nanoparticles with a brownish colour. Hernández *et al*. and Naaz *et al*. stated that magnesium ferrite ($MgFe_2O_4$) nanoparticles have a brownish to blackish colour [37-38]. This colour may vary depending on the synthesis method used. The yield of $MgFe_2O_4$ nanoparticles obtained was 70%.

3.2 Characteristics of $MgFe_2O_4$ Nanoparticles

Figure 3 shows the diffraction pattern of $MgFe_2O_4$ with diffraction peaks appearing at 2θ = 30.5°, 35.73°, 43.1°, 57.34°, and 62.98°, which correspond to field index values of (220), (311), (400), (511) and (440), which describes $MgFe_2O_4$

Figure 2. $MgFe_2O_4$ Nanoparticles

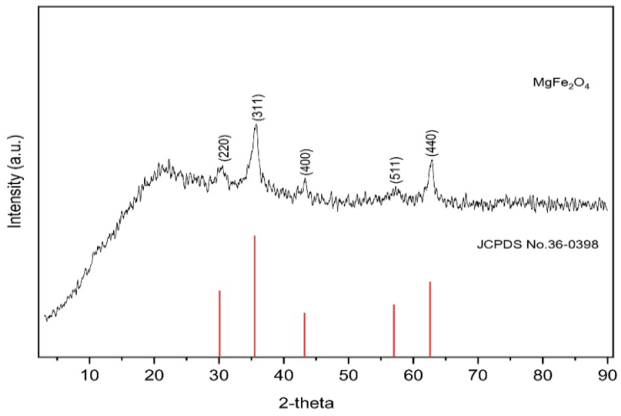

Figure 3. Diffraction pattern of $MgFe_2O_4$ nanoparticles

with spinel-type structure. The diffraction peak values of $MgFe_2O_4$ synthesized in this study have similarities with $MgFe_2O_4$ from JCPDS No. 36-0398 data.

The FWHM value must be significant to determine the small crystal size. The Debye-Scherer equation describes the relationship between crystal size and FWHM [39]. The Debye Scherrer equation states that the resulting crystal size value is inversely proportional to the FWHM value which influenced by the intensity of each crystal surface, where the higher the intensity, the smaller the FWHM value [40]. The results of determining the crystal size using the Debye-Scherrer equation show that $MgFe_2O_4$ nanoparticles have an average crystal size of 3.87 nm, which belongs to the nanocrystal group. Hydroxyl groups from flavonoids and polyphenols contained in pumpkin seed extract play an essential role as a capping agent in controlling crystal size by attaching to the crystal surface due to electrostatic forces so that it can help crystal growth and affect the properties of the resulting material [25]. Capping agents can affect crystal size by inhibiting crystal growth, resulting in crystals with smaller sizes [41].

Figure 4 shows that the morphology of the synthesized $MgFe_2O_4$ nanoparticles is spherical. Furthermore, the average particle size of $MgFe_2O_4$ nanoparticles was measured using Image J software (Figure 5). Figure 5 shows the size distribution of $MgFe_2O_4$ nanoparticles ranging from 5 - 90 nm, with the most dominant average particle size of 29 nm which belongs to the nanoparticle group.

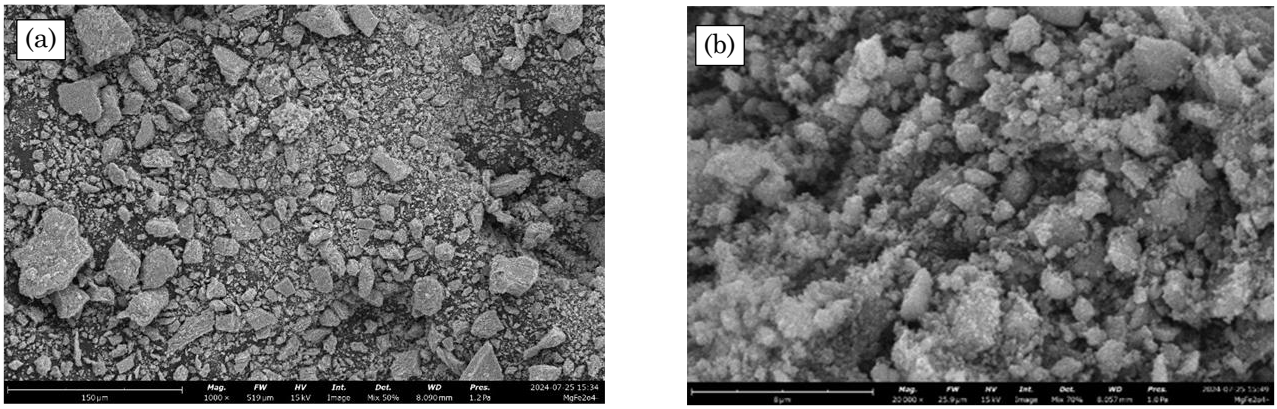

Figure 4. SEM analysis results of $MgFe_2O_4$ nanoparticles at magnification (a). 1.000×; and (b). 30.000×

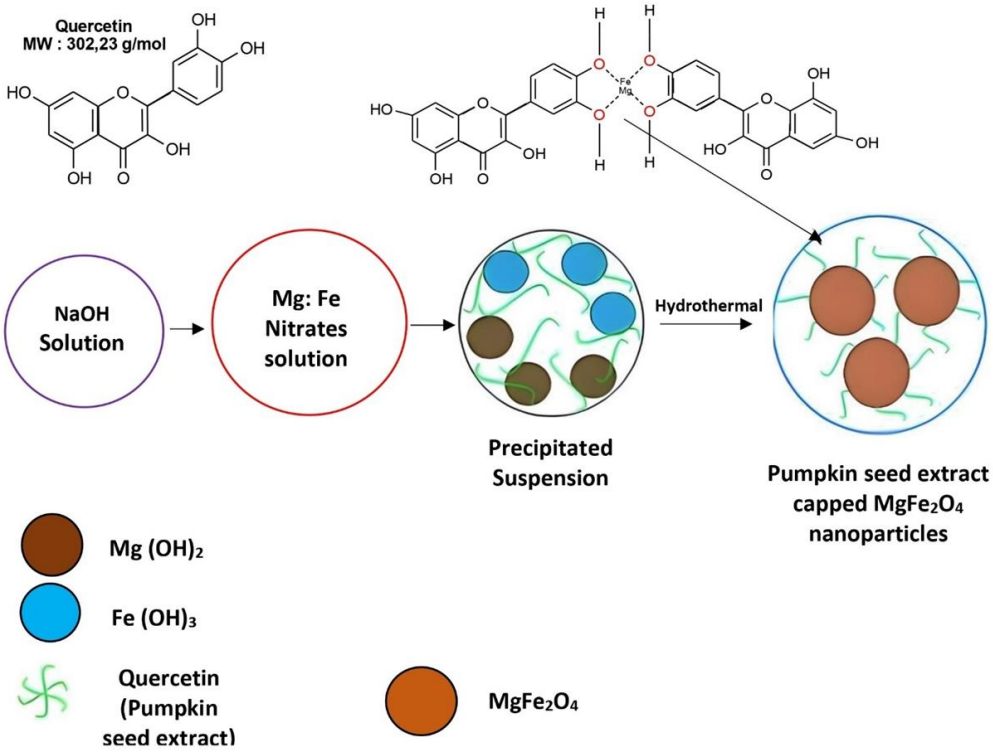

Figure 1. Mechanism of $MgFe_2O_4$ nanoparticles synthesis using pumpkin seed extract (*C. moschata*)

Figure 6 and Table 1 indicates that the synthesized $MgFe_2O_4$ nanoparticles are primarily composed of atomic oxygen (O), magnesium (Mg), and iron (Fe), with weight percentages of 8.7%, 25.8%, and 65.5%, respectively. The dominance of the Fe element over Mg and O is due to the 2:1 mole ratio of Fe to Mg in the synthesis of $MgFe_2O_4$. The EDX analysis confirms the absence of any impurities, reinforcing the high purity of the $MgFe_2O_4$ nanoparticles and the reliability of our research.

The band gap energy value can be determined using the Kubelka-Munk equation. The data entered are the wavelength and the percent reflectance value. The amount of band gap energy from UV-VIS DRS characterization is plotted on a Tauc-plot graph between $[F(R)hv]^2$ and energy (eV) (Figure 7). The Figure 7 shows the measurement results of the graph connecting the horizontal axis (eV) and the vertical axis $[F(R)hv]^2$. Figure 7 shows the band gap energy of $MgFe_2O_4$ nanoparticles produced is 1.94 eV. Rathinavel *et al.* [42] explained that the standard band gap energy of $MgFe_2O_4$ nanoparticles ranges from 1.9 eV to 2.1 eV. The resulting band gap energy value is the same as the research of Riyanti *et al.* and Aliyan *et al.* which is 1.9 eV [36,43]. The low band gap energy value allows $MgFe_2O_4$ nanoparticles to be effective in the visible light region [43]. The smaller the band gap energy, the greater the range of light that can be absorbed and the more effective in exciting electrons from the valence band to the conduction band, which has an impact on the number of radical species that can degrade dyes [21].

Table 1. Elemental composition in $MgFe_2O_4$ nanoparticles

Element	Composition (% w/w)
Oxygen (O)	8.7
Magnesium (Mg)	25.8
Iron (Fe)	65.5

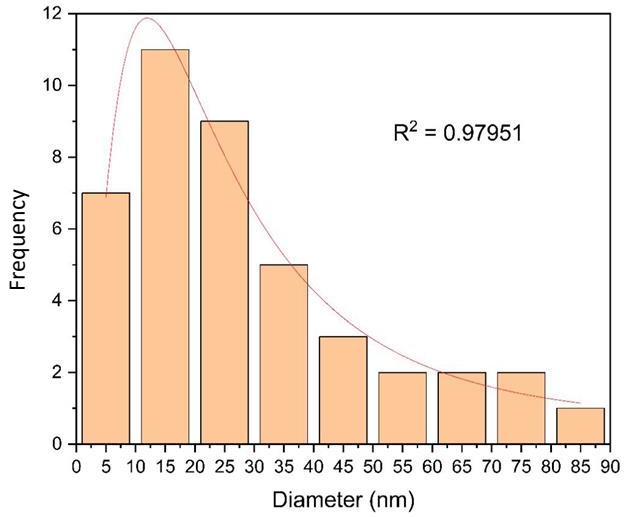

Figure 5. Particle size distribution of $MgFe_2O_4$ nanoparticles

3.3 Photocatalytic Activity of $MgFe_2O_4$ Nanoparticles

3.3.1 The Effect of pH

The effect of pH was analyzed under the reaction conditions of methylene blue pH = 6 - 13. The test results can be seen in (Figure 8). The photocatalytic activity of $MgFe_2O_4$ in degrading methylene blue was found to increase at pH = 6 - 13 (Figure 8a). The optimum condition was achieved at solution pH = 12, resulting in a degradation efficiency of 94.64% and a degradation capacity of 53.88 mg/g (Figure 8b). It is crucial to understand that the pH of the solution significantly affects the photodegradation process, as it directly influences the formation of hydroxyl radicals. These radicals, specifically hydroxyl radicals (HO•), are essential in the oxidation of methylene blue. The more hydroxyl radicals formed, the more methylene blue can be degraded.

In addition, the ability of the photocatalyst to degrade dyes depends on the interaction between $MgFe_2O_4$ and methylene blue. The pH of the solution dramatically affects the interaction strength of the photocatalyst and the dye. Methylene blue as a cationic dye can interact

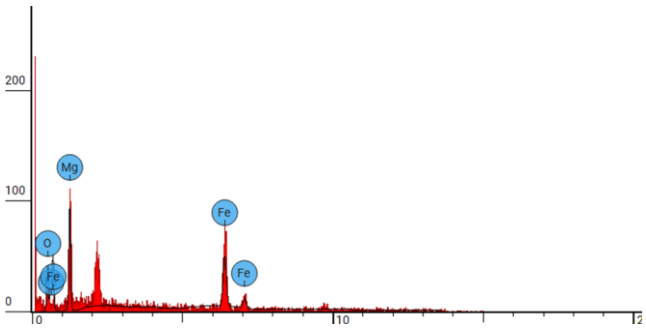

Figure 6. EDX graph of $MgFe_2O_4$

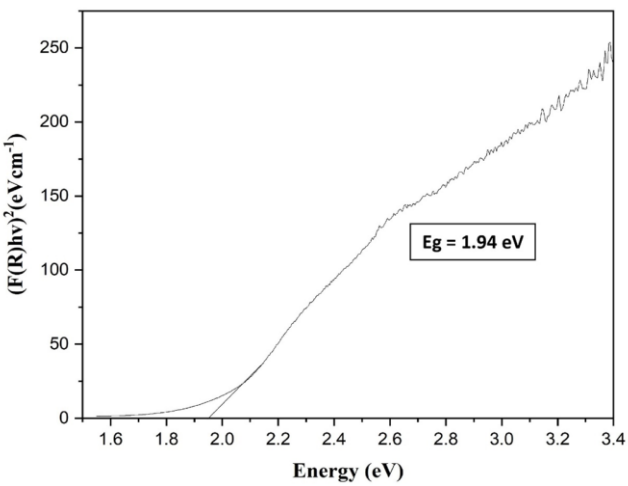

Figure 7. Band gap energy value of $MgFe_2O_4$ nanoparticles

through electrostatic interactions with the negatively charged catalyst surface [44-47].

The lowest degradation efficiency was achieved at pH = 6 of 9.22%. It is because, at acidic pH, the surface of $MgFe_2O_4$ is protonated by H^+ ions so that it tends to be positively charged and reduces its adsorption ability to methylene blue [48]. Meanwhile, in alkaline conditions ranging at pH = 8, 9, 10, 11, 12, and 13, the degradation efficiency was obtained at 9.43%, 33.66%, 10.96%, 55.32%, 94.64%, and 98.93%, respectively. Increasing the pH value (alkaline conditions) causes the photocatalyst surface to be negatively charged due to increased OH^- ions in the solution. This causes the electrostatic interaction between methylene blue, which tends to be positively charged, and the photocatalyst surface, which tends to be negatively charged, to increase. The more MB molecules interact with the photocatalyst, the more MB molecules are degraded.

The photocatalytic activity of $MgFe_2O_4$ continues to increase the degradation efficiency in the pH range of 11, 12, and 13, namely 55.32%, 94.64%, and 98.93%, respectively (Figure 8a). A key aspect of this process is the role of hydroxyl radicals (•OH), active species that play a significant role in the degradation of methylene blue pollutants. Photolysis tests produced degradation efficiencies of 15.7%, 26.6%, and 73.58% at pH of 11, 12 and 13, respectively (Figure 8a). The photolysis test results (Figure 8a) show that the optimum conditions are at pH = 12 with a degradation efficiency of 94.64%. This is because during the photolysis test, the degradation efficiency obtained was only 26.6%, so the increase in degradation efficiency when the $MgFe_2O_4$ photocatalyst was added was 68.04%. While at pH = 13, the increase in degradation efficiency is only around 25.35%. Figure 8a also shows that methylene blue is degraded by $MgFe_2O_4$ through a photocatalytic degradation mechanism. This can be seen from the test results in dark conditions at pH = 11 showing a difference where MB was degraded by 55.32% in light conditions and 17.22% in dark conditions.

3.3.2 The Effect of Methylene Blue Initial Concentration

This test was conducted to observe the effect of the initial methylene blue concentration on the photocatalytic activity of $MgFe_2O_4$. This test was carried out by dispersing 25 mg of $MgFe_2O_4$ nanoparticles into 50 mL of pH = 12. The photocatalyst concentration variation test results can be seen in (Figure 9). Figure 8 illustrates that the photocatalytic activity of $MgFe_2O_4$ nanoparticles in degrading methylene blue reached an optimal condition at a methylene blue concentration of 60 ppm, with a degradation efficiency of 78.09% (Figure 9a) and a degradation capacity of 94.28 mg/g (Figure 9b). Notably, the efficiency decreased at higher concentrations, a significant finding that aligns with the work of Nikazar *et al.* who reported a similar trend [49].

The decrease in degradation efficiency occurs because the photocatalyst experiences saturation due to the high concentration of methylene blue that covers the surface of the photocatalyst, thus reducing the intensity of light hitting the surface of the photocatalyst, which results in the inhibition of electron excitation in the process of free radical formation. Makofane *et al.* (2021) stated that the inhibition of the electron excitation process causes inhibition of the formation of hydroxyl radicals (•OH) and superoxide radicals ($•O_2^-$), which play a role in degrading methylene blue [50].

The highest degradation efficiency was obtained at a concentration of 10 ppm at 98.16% but had a lower degradation capacity than the concentration of 60 ppm, which was 18.52 mg/g (Figure 9b). This is because the number of dye molecules that react with the active side of the catalyst is less, resulting in a smaller degradation capacity value despite the high degradation

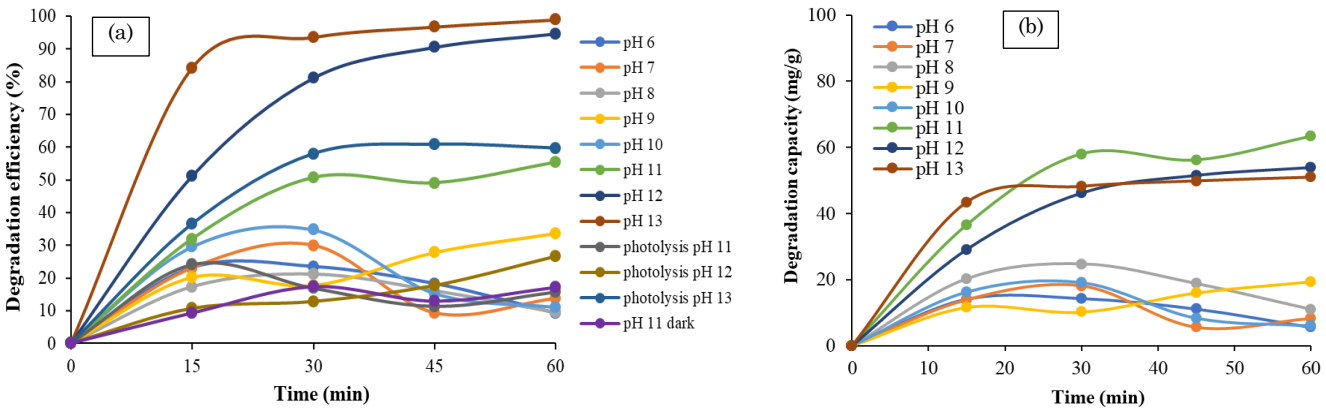

Figure 8. Photocatalytic activity of $MgFe_2O_4$ with pH variation (a) degradation efficiency; (b) degradation capacity at MB concentration 30 mg/L and catalyst dosage of 0.05%

efficiency. The mechanism of methylene blue photodegradation with the help of the $MgFe_2O_4$ catalyst is written in the following Equations 13-18:

$$MgFe_2O_4 + hv \rightarrow MgFe_2O_4\,(e^-) + MgFe_2O_4\,(h^+) \quad (13)$$
$$MgFe_2O_4\,(e^-) + O_2 \rightarrow \bullet O_2^- \quad (14)$$
$$H_2O + \bullet O_2^- \rightarrow \bullet OH + OH^- \quad (15)$$
$$MgFe_2O_4\,(h^+) + OH^- \rightarrow \bullet OH \quad (16)$$
$$MgFe_2O_4\,(h^+) + H_2O \rightarrow \bullet OH + H^+ \quad (17)$$
$$\bullet OH + \text{methylene blue} \rightarrow \text{Degraded product} \quad (18)$$

The $MgFe_2O_4$ photocatalyst, when exposed to UV light, excites electrons from the valence band to the conduction band, forming excited electron pairs (e^-) in the conduction band and electron holes (h^+) in the valence band (Equation 13). The excited electrons react with oxygen (O) molecules on the photocatalyst surface to form superoxide anion radicals ($\bullet O_2^-$) (Equation 14). The anion reacts with water molecules (H_2O) adsorbed on the catalyst surface to produce hydroxyl radicals ($\bullet OH$) and hydroxide ions (OH^-) (Equation 15). hydroxide ions (OH^-) react with electron holes (h^+) to form hydroxyl radicals ($\bullet OH$) (Equation 16) which are potent oxidizing agents. Meanwhile, electron holes (holes) react with H_2O to produce hydroxyl radicals ($\bullet OH$) and H^+ ions (Equation 17). It is the hydroxyl radicals ($\bullet OH$) that play a key role in degrading the methylene blue compound of the dye, demonstrating the effectiveness of the process and producing degradation products in the form of CO_2, H_2O, and mineral acids (Equation 18) [15,51]. Abdollahi *et al.* explained that hydroxyl radicals have a high level of reactivity in oxidizing dyes. The greater the hydroxyl radical content, the greater the photodegradation process and the amount of degraded dye [52].

3.3.3 The Effect of $MgFe_2O_4$ Mass

Figure 10a shows that the methylene blue degradation efficiency increases as the mass of the $MgFe_2O_4$ catalyst rises from 5 mg to 25 mg. Despite the increase in percent degradation, the highest degradation capacity was achieved at the 5 mg photocatalyst mass, which amounted to 391.98 mg/g (Figure 10b). Therefore, a mass of 5 mg $MgFe_2O_4$ was chosen as the optimum catalyst for degrading methylene blue.

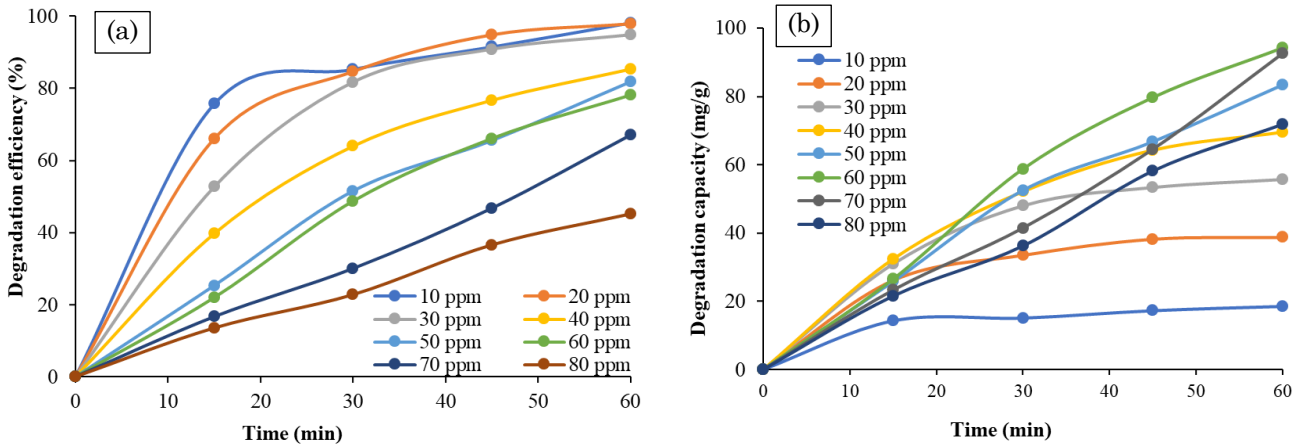

Figure 9. Photocatalytic activity of $MgFe_2O_4$ varying methylene blue concentration (a) degradation efficiency; (b) degradation capacity at pH = 12 and catalyst dosage of 0.05%

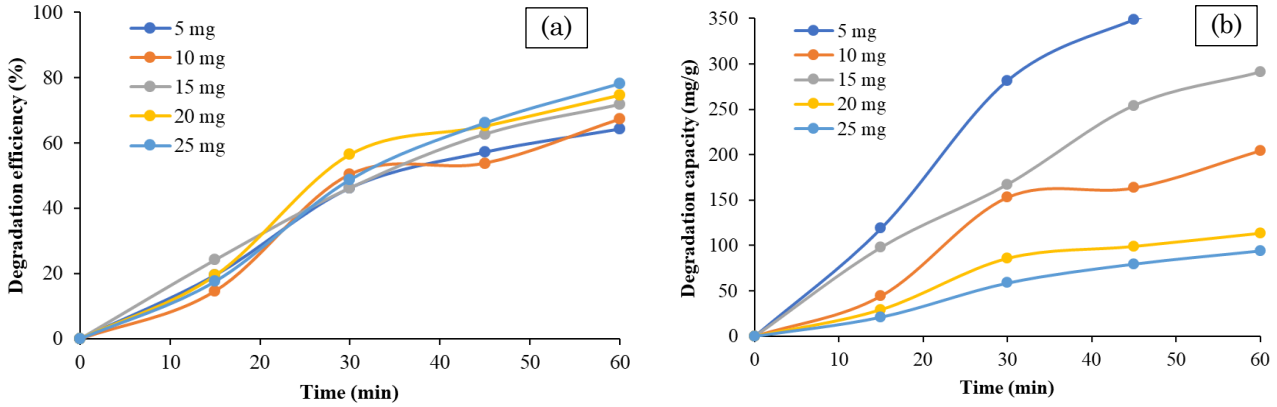

Figure 10. Photocatalytic activity of $MgFe_2O_4$ photocatalyst mass variation (a) degradation efficiency; (b) degradation capacity at MB concentration 60 mg/L and pH of 12

Increasing the number of photocatalysts leads to an increase in the number of active sites on the photocatalyst surface. It increases the formation of hydroxyl radicals (•OH) that play a role in the dye degradation process. In addition, the efficiency degradation of $MgFe_2O_4$ on different types of dyes is listed in Table 2. The $MgFe_2O_4$ produced in this study has an excellent degradation activity towards methylene blue dye with a less reaction time.

4. Conclusions

$MgFe_2O_4$ nanoparticles synthesized by adding 3 mL of pumpkin seed extract have a nanoscale crystal size with an average crystal size of 3.87 nm, a cubic spinel structure with an average particle size of 29 nm and a band gap energy value of 1.94 eV. The $MgFe_2O_4$ nanoparticles produced were able to degrade methylene blue with the highest degradation efficiency of 64.20% and degradation capacity of 391.98 mg/g at a photocatalyst mass of 5 mg, 50 mL of methylene blue concentration of 60 ppm, and pH = 12 for 60 minutes.

Acknowledgment

The authors wish to thank Pusat Laboratorium Terpadu (PLT) Universitas Islam Negeri (UIN) Syarif Hidayatullah Jakarta for facilitating this work.

CRediT Author Statement

Dede Sukandar: Supervision; Adawiah: writing, editing and reviewing; Shella Fitria: Formal analysis, investigation, writing original draft; Nanda Saridewi: supervision; Salman Farishi; Supervison; Nurhasni Nurhasni: Supervision; Saeful Rohman: Supervision; Isalmi Aziz: Supervision; Yulyani Nur Azizah: Supervision.

Declaration of Competing Interest

The authors declare that they have no known competing financial interests or personal relationships that could have appeared to influence the work reported in this paper.

References

[1] Nunes, D., Pimentel, A., Santos, L., Barquinha, P., Pereira, L., Fortunato, E., & Martins, R. (2019). Synthesis, design, and morphology of metal oxide nanostructures. *In Metal Oxide Nanostructures*. DOI: 10.1016/b978-0-12-811512-1.00002-3

[2] [BPS] Badan Pusat Statistik. (2021). Statistik Indonesia. Jakarta : BPS.

[3] Allouche, F.N., & Yassaa, N. (2018). Potential adsorption of methylene blue from aqueous solution using green macroalgaePosidonia oceanica. *IOP Conference Series: Materials Science and Engineering*, 323(1). DOI: 10.1088/1757-899X/323/1/012006

[4] Koyuncu, H., & Kul, A. R. (2020). Removal of methylene blue dye from aqueous solution by nonliving lichen (*Pseudevernia furfuracea* (L.) Zopf.), as a novel biosorbent. *Appl. Water Science*, 10, 72. DOI: 10.1007/s13201-020-1156-9

Table 2. Comparison of the degradation efficiency of $MgFe_2O_4$ in different dyes

Synthesis method	Dye	Conditions	Degradation efficiency (%)	References
Sol-gel	Bromothymol Blue (BB)	Under solar light irradiation, BB concentration of 10 mg/L, t = 180 min, pH = 3 and	65	[53]
Microwave solution combustion (Msc)	Rb21	Under visible lighting (two 9 W LED bulbs), Halonix source irradiation, Rb21 concentration of 20 mg/L, t = 180 min, pH = 7	93	[54]
Co-precipitation	Carbol fuchsin (CF)	Under UV irradiation, pH = 9, CF concentration = 10 mg/L, t = 135 min	96	[55]
Co-precipitation	Congo red	Under visible light irradiation (150 w Xenon lamp), Congo red concentration of 10 mg/L, pH of 6, H_2O_2 concentration of 2.5 mM, and t = 180 min.	99.62	[27]
Hydrothermal	Methylene blue (MB)	Under visible light irradiation (250 w mercury lamp), MB concentration of 30 mg/L, pH of 12, and t = 60 min	94.64	This work

[5] Ceccaroli, B., & Lohne, O. (2011). Solar Grade Silicon Feedstock. *In Handbook of Photovoltaic Science and Engineering, Second Edition* (pp.169 - 217) (Issue October 2010). DOI: 10.1002/9780470974704.ch5

[6] Saeed, M., Usman, M., & Haq, A. ul. (2018). Catalytic Degradation of Organic Dyes in Aqueous Medium. *Photochemistry and Photophysics - Fundamentals to Applications*. DOI: 10.5772/intechopen.75008

[7] Kumar, P. S., Ramalingam, S., & Sathishkumar, K. (2011). Removal of methylene blue dye from aqueous solution by activated carbon prepared from cashew nut shell as a new low-cost adsorbent. *Korean Journal of Chemical Engineering*, 28(1), 149–155. DOI: 10.1007/s11814-010-0342-0

[8] Wang, P., Cao, M., Wang, C., Ao, Y., Hou, J., & Qian, J. (2014). Kinetics and thermodynamics of adsorption of methylene blue by a magnetic graphene-carbon nanotube composite. *Applied* Surface Science, 290, 116–124. DOI: 10.1016/j.apsusc.2013.11.010

[9] Putra, R.A., Alamsyah, W., & Indrayana, I.P.T. (2019). Characterization of microstructural and optical properties of $MgFe_2O_4$ nanoparticles for photocatalyst of mercury (Hg). *Jurnal Neutrino: Jurnal Fisika dan Aplikasinya*, 11(1): 1–5. DOI: 10.18860/neu.v11i1.5531

[10] Kumari, H., Sonia, Suman, Ranga, R., Chahal, S., Devi, S., Sharma, S., Kumar, S., Kumar, P., Kumar, S., Kumar, A., & Parmar, R. (2023). A review on photocatalysis used for wastewater treatment: dye degradation. *In Water, Air, and Soil Pollution*, 234, 6. DOI: 10.1007/s11270-023-06359-9

[11] Zahro, S.F., & Adityosulindro, S. (2023). Literature review: penggunaan bahan berbasis limbah sebagai adsorben untuk degradasi zat warna pada air limbah. *Jurnal Kesehatan Lingkungan Indonesia*, 22(3), 359–368. DOI: 10.14710/jkli.22.3.359-368

[12] Gopi, V., Upgade, A., & Soundararajan, N. (2012). bioremediation potential of individual and consortium non-adapted fungal strains on azo dye containing textile effluent. *Pelagia Research Library*. 3(1), 303–311.

[13] Xue, C.Q., Zhang, J., Li, X., Chou, W., Zhang, H., Ye, Z., Cui. & Dobson, P.J. (2013). High photocatalytic activity of Fe_3O_4-SiO_2-TiO_2 functional particles with core-shell structure. *Journal of Nanomaterials*. 1-8. DOI: 10.1088/1742-6596/1595/1/012003

[14] Yang, X., & Wang, D. (2018). Photocatalysis: from fundamental principles to materials and applications [review-article]. *ACS Applied Energy Materials*, 1(12), 6657–6693. DOI: 10.1021/acsaem.8b01345

[15] Madhu, G.M., Raj, M.A.L.A., Pai, K.V.K., & Rao, S. (2007). Photodegradation of methylene blue dye using UV/ $BaTiO_3$, UV/H_2O_2, and UV/ H_2O_2/ $BaTiO_3$ oxidation processes, *Indian Journal of Chemical Technology*. 14, 139–144.

[16] Al-Nuaim, M.A., Alwasiti, A.A., & Shnain, Z.Y. (2023). The photocatalytic process in the treatment of polluted water. *Chemical Papers*, 77(2), 677–701. DOI: 10.1007/s11696-022-02468-7

[17] Aritonang, A.B., Parwaty, P., Wibowo, M.A., Ardiningsih, P., & Adhitiyawarman, A. (2023). Sintesis TiO_2-rGO dengan pereduksi alumunium untuk fotokatalisis degradasi metilen biru dibawah irradiasi sinar tampak. *Equilibrium Journal of Chemical Engineering*, 6(2), 150. DOI: 10.20961/equilibrium.v6i2.65518

[18] Wardhani, N. (2014). Fotokatalis TiO_2-zeolit untuk degradasi metilen biru. *Chemistry Progress*, 7(1), 9–14. DOI: 10.35799/cp.7.1.2014.4848

[19] Garg, V. K., Sharma, V. K., & Kuzmann, E. (2016). Purifcation of water by ferrites-mini review. *ACS Symposium Series*, 1238 (Figure 1), 137–143. DOI: 10.1021/bk-2016-1238.ch005

[20] Kooti, M. & Sedeh, A.N. (2013). Synthesis and characterization of $NiFe_2O_4$ magnetic nanoparticles by combustion method. *Journal of Materials Science and Technology*. 29, 34-38. DOI: 10.1016/j.jmst.2012.11.016

[21] Shen, Y., Wu, Y., Li, X., Zhao, Q., & Hou, Y. (2013). One-pot synthesis of $MgFe_2O_4$ nanospheres by solvothermal method. *Materials Letters*. 96, 85–88. DOI: 10.1016/j.matlet.2013.01.023

[22] Sripriya, R.C., Mahendiran, M., Madahavan, J., & Victor Antony Raj, M. (2019). Enhanced magnetic properties of $MgFe_2O_4$ nanoparticles. *Materials Today: Proceedings*, 8, 310–314. DOI: 10.1016/j.matpr.2019.02.116

[23] Kaur, N., & Kaur, M. (2014). Comparative studies on impact of synthesis methods on structural and magnetic properties of magnesium ferrite nanoparticles. *Processing and Application of Ceramics*. 8(3), 137–143. DOI: 10.2298/PAC1403137K

[24] Tariq, A., Ullah, U., Ahmad, I., Asif, M., Sadiq, I., & Haleem, H. (2019). Comparative analysis of the magnesium ferrite ($MgFe_2O_4$) nanoparticles synthesised by three different routes. *IET Nanobiotechnology*, 13(7), 697–702. DOI: 10.1049/iet-nbt.2018.5032

[25] Saridewi, N., Syaputro, H.T., Aziz, I., Dasumiati, & Kumila, B.N. (2021). Synthesis and characterization of ZnO nanoparticles using pumpkin seed extract (*Cucurbita moschata*) by the sol-gel method. *AIP Conference Proceedings*, 9, 7–12. DOI: 10.1016/j.matpr.2019.02.029

[26] Saridewi, N., Komala, S., Zulys, A., Nurbayti, S., Tulhusna, L., & Adawiah, A. (2022). Synthesis of ZnO-Fe_3O_4 magnetic nanocomposites through sonochemical methods for methylene blue degradation. *Bulletin of Chemical Reaction Engineering & Catalysis*, 17(3), 650–660. DOI: 10.9767/bcrec.17.3.15492.650-660

[27] Riyanti, F., Nurhidayah, Purwaningrum, W., Yuliasari, N., & Hariani, P.L. (2023). $MgFe_2O_4$ magnetic catalyst for photocatalytic degradation of congo red dye in aqueous solution under visible light irradiation. *Environment and Natural Resources Journal*, 21(4), 322–332. DOI: 10.32526/ennrj/21/20230002

[28] Saridewi, N., Utami, J.D., Zulys, A., Nurbayti, S., Nurhasni, N., Adawiah, A., Putri, R.A., & Kamal, R., (2024). Utilization of lidah mertua (*Sansevieria trifasciata*) extract for green synthesis of $ZnFe_2O_4$ nanoparticle as visible-light responsive photocatalyst for dye degradation. *Case Studies in Chemical and Environmental Engineering*, 9, 100745. DOI: 10.1016/j.cscee.2024.100745

[29] Meng, L.Y., Wang, B., Ma, M.G., & Lin, K.L. (2016). The progress of microwave-assisted hydrothermal method in the synthesis of functional nanomaterials. *Materials Today Chemistry*, 1–2, 63–83. DOI: 10.1016/j.mtchem.2016.11.003

[30] Yuliarto, B., Septiani, N.L.W., Kaneti, Y.V., Iqbal, M., Gumilar, G., Kim, M., Na, J., Wu, K. C.W., & Yamauchi, Y. (2019). Green synthesis of metal oxide nanostructures using naturally occurring compounds for energy, environmental, and bio-related applications. *New Journal of Chemistry*, 43(40), 15846–15856. DOI: 10.1039/c9nj03311d

[31] Javed, R., Usman, M., Tabassum, S., & Zia, M. (2017). Effect of capping agents: Structural, optical and biological properties of ZnO nanoparticles. *Applied Surface Science*, 386, 319–326. DOI: 10.1016/j.apsusc.2016.06.042

[32] Jiwatami, A.M.A. (2022). Aplikasi termokopel untuk pengukuran suhu autoklaf. *Lontar Physics Today*, 1(1), 38–44. DOI: 10.26877/lpt.v1i1.10695

[33] Lestari, W.W., Hartono, J., Wulansari, D.W.T., Pramuja, E., Azhari, F., & Kusumaningsih, T. (2023). Pengaruh metode sintesis secara solvo-hidrotermal dan elektrokimia terhadap morfologi struktur HKUST-1 sebagai katalis heterogen dalam reaksi esterifikasi asam palmitat. *ALCHEMY Jurnal Penelitian Kimia*, 19(1), 1. DOI: 10.20961/alchemy.19.1.62466.1-13

[34] Rohmah, D.P.M., Hadi, S., & Baktir, A. (2019). Pemurnian parsial dan kritalisasi papain dari getah *Carica papaya*. *Jurnal Kimia Riset*, 4(2), 152–160. DOI: 10.20473/jkr.v4i2.16902

[35] Puspitasari, P., Muhammad, A., Suryanto, H., & Andoko. (2028). Magnetic properties of manganese ferrite ($MnFe_2O_4$) by co-precipitation method with different pH concentration. *High Temperature Material Processes an International Quarterly of High-Technology Plasma Processes*, 22 (4), 239–248. DOI: 10.1615/HighTempMatProc.2018029155

[36] Tournebize, J., Boudier, A., Joubert, O., Eidi, H., Bartosz, G., Maincent, P., Leroy, P., Sapin-Minet, A. (2012). Impact of gold nanoparticle coating on redox homeostasis. *International Journal of Pharmaceutics*, 438(1-2), 107-16. DOI: 10.1016/j.ijpharm.2012.07.026

[37] Reséndiz-Hernández, P.J., de Hoyos-Sifuentes, D.H., Reséndiz-Flores, E.O., Ochoa-Palacios, R.M. & Altamirano-Guerrero, G. (2023). Synthesis of pure $MgFe_2O_4$ nanoparticles: an intelligent prediction approach and experimental validation, *Journal of Sol-Gel Science and Technology*. 107, 620–628. DOI: 10.1007/s10971-023-06168-w

[38] Naaz, F., Dubey, H.K., Kumari, C., & Lahiri, P. (2020). Structural and magnetic properties of $MgFe_2O_4$ nanopowder synthesized via co-precipitation route. *SN Applied Sciences*, 2(5), 1–8. DOI: 10.1007/s42452-020-2611-9

[39] Didik, L.A. (2020). Penentuan ukuran butir kristal $CuCr_{0,98}Ni_{0,02}O_2$ dengan Menggunakan X-Ray Difraction (XRD) dan Scanning Electron Microscope (SEM). *Indonesian Physical Review*. 3(1), 6–14. DOI: 10.29303/ipr.v3i1.37

[40] Masruroh., Manggara, B.A., Lapailaka, T., & Tjahjanto, T.R. (2013). Penentuan ukuran kristal (*crystallite size*) lapisan tipis PZT dengan metode XRD melalui pendekatan persamaan Debye Scherrer, *Journal of Educational Innovation*. 1(2). DOI: 10.18551/erudio.1-2.4

[41] Prabhakaran, T., Mangalaraja, R.V., Denardin, J.C., & Varaprasad, K. (2018). The effect of capping agents on the structural and magnetic properties of cobalt ferrite nanoparticles. *Journal of Materials Science*: *Materials in Electronics*, 29(14), 11774–11782. DOI: 10.1007/s10854-018-9276-9

[42] Rathinavel, S., Deepika, R., Dhananjaya, P. and Manikandan, A. (2020). Synthesis and characterization of $MgFe_2O_4$ and $MgFe_2O_4$/rGO nanocomposites for the photocatalytic degradation of methylene blue. *Inorganic and Nano-Metal Chemistry*. 2(1), 1-9. DOI: 10.1080/24701556.2020.1771590

[43] Aliyan, N., Mirkazemi, S.M., Masoudpanah, S. M. & Akhari, S. (2017). The effect of post-calcination on cation distributions and magnetic properties of the coprecipitated $MgFe_2O_4$ nanoparticles. *Applied Physics A Material Science and Processing*. 2(1), 446-503. DOI: 10.1007/s00339-017-1053-8

[44] Cheng, M., Zeng, G., Huang, D., Lai, C., Wei, Z., Li, N., Xu, P., Zhang, C., Zhu, Y., & He, X. (2015). Combined biological removal of methylene blue from aqueous solutions using rice straw and *Phanerochaete chrysosporium*. *Applied Microbiology and Biotechnology*, 99(12), 5247–5256. DOI: 10.1007/s00253-014-6344-9

[45] Eljiedi, A. A. A. & Kamari, A., (2017). Removal of methyl orange and methylene blue dyes from aqueous solution using lala clam (*Orbicularia orbiculata*) shell. *AIP Conf. Proc.*, 1847(1): 40003. DOI: 10.1063/1.4983899

[46] Wang, S. & Zhu, Z. (2007). Effects of acidic treatment of activated carbons on dye adsorption. *Dye. Pigment.*, 75, 306-314, DOI: 10.1016/j.dyepig.2006.06.005

[47] Umpuch, C. & Sakaew, S., (2013). Removal of methyl orange from aqueous solutions by adsorption using chitosan intercalated montmorillonite. *Songklanakarin Journal of Science and Technology,* 35(4), 451-459.

[48] Permata, G. D., Diantariani, P. N., & Widihati, G. A. I. (2016). Degradasi fotokatalitik fenol menggunakan fotokatalis ZnO dan sinar UU. *Jurnal Kimia*, 10(2), 263-269. DOI: 10.24843/jchem.2016.v10.i02.p13

[49] Nikazar, M., Gholivand, K., & Mahanpoor, K. 2007. Using TiO_2 supported on clinoptilolite as a catalyst for photocatalytic degradation of azo dye disperse yellow 23 in water. *Kinetics and Catalysis*. 48(2), 214-220. DOI: 10.1134/S002315840702005X

[50] Makofane, A., Motaung, D.E., & Hintsho-mbita, N.C. (2021). Photocatalytic degradation of methylene blue and sulfisoxazole from water using biosynthesized zinc ferrite nanoparticles. *Ceramics International,* 47 (16), 22615-22626. DOI: 10.1016/j.ceramint.2021.04.274

[51] Dong, H., Zeng, G., Tang, L., Fan, C., Zhang, C., He, X., He, Y. 2015. An overview on limitations of TiO_2-based particles for photocatalytic degradation of organic pollutants and the corresponding countermeasures. *Water Research*. 79, 128–146. DOI: 10.1016/j.watres.2015.04.038

[52] Abdollahi, Y., Abdullah, A.H., Zainal, Z., Yusof, N.A. (2011). Photodegradation of M-cresol by zinc oxide under visible-light irradiation. *International Journal of Molecular Sciences*. 13(1), 302-15. DOI: 10.3390/ijms13010302

[53] Soukeur, A., Kaci, M.M., Omeiri, S., Bellal, B., Amara, M., & Trari, M. (2023). Photocatalytic degradation of bromothymol blue over $MgFe_2O_4$ under sunlight exposure. *Optical Materials*. 142 (2023) 114108. DOI: 10.1016/j.optmat.2023.114108

[54] Jarariya, R., & Suresh, K. (2023). Spinel ferrite nanomaterials- $MgFe_2O_4$- Synthesis by appropriate microwave solution combustion (MSC) method of visible light–responsive photocatalyst for Rb21 dye degradation. *Materials Today: Proceedings*. 72 (2023), 2618–2629. DOI: 10.1016/j.matpr.2022.07.393

[55] El Khawaga, A.M., Ayman, M., Hafez, O., & Shalaby, R.E. (2024). Photocatalytic, antimicrobial and antibiofilm activities of $MgFe_2O_4$ magnetic nanoparticles. *Scientific Reports*. 14 (2024) 12877. DOI: 10.1038/s41598-024-62868-5